77th IIW Annual Assembly and International Conference on Welding and Joining 7-12 July 2024 Rhodes, Greece

Characterization of welds in copper generated by a high-power blue laser

Sean Shi Hao Teoh[1,2], *Pratik* Shukla[3], *Ioannis* Metsios[4], *Sanjay* Gupta[5], *Naien* Wu[6], *Aurelie* Tolten[3], and *Wei* Zhou[1,2*]

[1]Singapore Centre for 3D Printing, School of Mechanical and Aerospace Engineering, Nanyang Technological University, 50 Nanyang Avenue, 639798, Singapore
[2]School of Mechanical and Aerospace Engineering, Nanyang Technological University, 50 Nanyang Avenue, 639798, Singapore
[3]The Manufacturing Technology Centre, Ansty Park, Coventry CV7 9JU, United Kingdom
[4]Lumpi Ltd, 8a Sun Street, Potton, Sandy, England, SG19 2LR, United Kingdom
[5]W&H Factory Complex, Hay Mills, Fordrough, Small Heath, Birmingham B25 8DL, United Kingdom
[6]Precision Laser Solutions Pte. Ltd, 280 Woodlands Industrial Park E5, #09-39/40, 757322, Singapore

Abstract. High quality precision welding of copper has become increasingly important following the trends of electrification of automobiles and automation of manufacturing. Laser welding is a suitable technique to achieve precision copper welds, whether between copper or between copper and other materials. However, high quality welds can be difficult to attain because of copper's high reflectivity to infrared lasers and high thermal conductivity. This study characterizes line and spot welds created using a state-of-the-art 1.5 kW, 445 nm blue CW diode laser on 0.9 mm thick copper with 0.3 mm thick stainless steel. The results of the study showed that weld penetration depth, weld width, porosity and grain size are positively correlated with laser energy input. The presence of weld zones show that the use of relatively low-powered blue lasers can overcome the initial reflectivity of copper to infrared lasers but the observation of porosity in almost welds means that process parameter optimization remains important to achieve high quality welds.

1 Introduction

High quality precision welding of copper has become increasingly important following the trends of electrification of automobiles and automation of manufacturing. Within the domain of electric vehicles (EVs), batteries are one of the critical components that enable energy to be stored in EVs for propulsion when it is disconnected from the power grid.

Ideally, electrical power transported from the batteries to the rest of the EV should be done so efficiently with minimal energy loss via heat. In order to achieve this objective, electrical contact points between components should be joined properly with high electrical conductivity and good mechanical properties (e.g. hardness, shear strength, residual stress) [1]. These electrical contact points to be joined within battery assemblies could consist of dissimilar materials (often including copper because of its high electrical conductivity) [2]. The substrates are often of low thickness in the range of millimetres [2], and can be located close to other components that are of low melting points (e.g. polymers) or hazardous or explosive when heated (e.g. lithium). This presents new challenges for welding because welding requirements and joint quality outcomes both become more stringent.

To meet these requirements, laser welding is a particularly attractive technique because of its high precision, ease of automation and high energy intensity [3]. The laser's relatively small spot size allows excellent localisation of laser energy transfer onto the irradiated spot. Precise electronic control of energy being deployed in the process also allows penetration depth and thermal load of the battery assemblies to be controlled and limited to requirements. Finally, the non-contact nature of the process makes it possible to weld intricate structures with difficult access. However, high quality welds can be challenging to attain because of copper's high reflectivity to infrared lasers and high thermal conductivity [3]. The use of green or blue lasers is one way to mitigate the drawbacks of laser welding of copper. In this study, a continuous wave (CW) blue laser was used to weld copper plates to stainless steel plates and the welds were subsequently characterised in terms of their weld geometry, microstructure, grain size, defects, and hardness.

2 Materials and methods

A top-hat CW 1.5 kW blue diode laser (Laserline, LDMblue 1500-30, Germany) of 445 nm wavelength was used for experimental trials. A series of experiments comprising line welds (length = 29 mm) followed by spot welds were conducted, to weld 0.9 mm thick copper plates to 0.3 mm thick stainless steel plates in a lap joint configuration (Fig. 1). As both weld penetration and weld quality can be influenced by the fit up of the materials being welded, the copper and stainless steel plates were cleaned with ethanol and clamped tightly prior to welding.

For the line welds, the process parameters were the same. For the spot welds, laser welding experiments were conducted by changing the laser active time from 1 s to 0.125 s. The process parameters used for each weld characterized in this study are detailed in Table 1.

* Corresponding author: mwzhou@ntu.edu.sg or wzhou@cantab.net

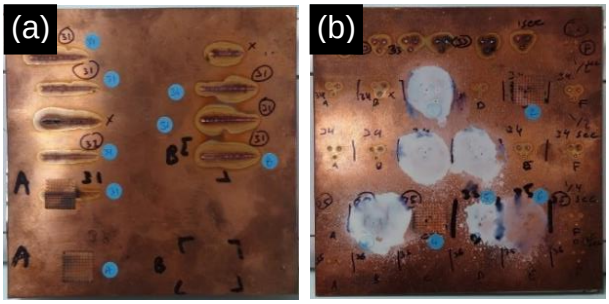

Fig. 1. 0.9 mm thick copper plate welded to 0.3 mm thick stainless steel plate. (a) Line welds; and (b) spot welds.

Table 1. Process parameters of the welds.

Sample	Laser power (kW)	Scan speed (mm/s)	Spot size ⌀ (mm)	Laser active time (s)
Line Weld 1 (LW1)	1.46	3	0.716	[2]9.667
Line Weld 2 (LW2)	1.46	3	0.716	[2]9.667
Spot Weld 1 (SW1)	1.46	0	0.716	1.000
Spot Weld 2 (SW2)	1.46	0	0.716	0.500
Spot Weld 3 (SW3)	1.46	0	0.716	0.250
Spot Weld 4 (SW4)	1.46	0	0.716	0.125

Table 2. Calculated parameters of the welds.

Sample	Laser intensity[3] (W/cm^2)	Laser energy per weld[4] (J)	Heat input density[5] (J/cm^2)
LW1	362,607.62	14,113.33	66,677.25
LW2	362,607.62	14,113.33	66,677.25
SW1	362,607.62	1,460.00	362,607.62
SW2	362,607.62	730.00	181,303.81
SW3	362,607.62	365.00	90,651.91
SW4	362,607.62	182.50	45,325.95

Because the plates were thin, mechanical cutting using a handheld hacksaw would cause deformation and delamination of layers while excessive heat generated from abrasive cutting may cause warping and affect the characterization results. Hence, wire electrical discharge machining (Troop, 8WPC-C, Taiwan) was used to extract the welds from the plates for characterization.

Cross-sections of welds were obtained using a micro-cutter equipped with a diamond blade (LAM PLAN, CUTLAM Micro 1.1, France). Metal strips were extracted perpendicular to the line welds, while metal strips were extracted tangential to the spot welds.

The cross-sections were mounted using a hot mounting press (LAM PLAN, PRESSLAM 1.1, France), ground and polished using silicon carbide sandpaper and diamond suspensions with a grinding and polishing machine (Struers, Laboforce-50, Denmark), and chemically etched using pre-mixed Kalling's reagent purchased from Best Chemical Co (S) Pte Ltd, Singapore.

Micrographs of the weld cross-sections were taken using a laser scanning confocal microscope (Lext, OLS4100, Japan) and a field emission scanning electron microscope (FESEM) (JEOL, JSM-7600, Japan). Electron backscatter diffraction (EBSD) images of the cross-sections were taken using an EBSD detector (Oxford Instruments / HKL Technology, Nordlys, United Kingdom / Denmark) fitted to the FESEM. For the spot welds, the EBSD image of only the first weld zone was obtained for comparison. Weld penetration depth and weld width were measured using the step measurement function in the Lext OLS4100 software of the laser scanning confocal microscope (Lext, OLS4100, Japan).

3 Results and discussion

3.1 Weld geometry

Out of the two line welds and four spot welds, only SW1 (Fig. 3c) penetrated to the stainless steel plate (weld penetration depth = 781 µm) and there was no melting of the stainless steel plate in this case. For the line weld samples, the weld penetration depth differed by 146 µm (Table 3) and weld width differed by 33 µm (Table 3) although the heat input density was the same at 66,677.25 J/cm^2 (Table 2). For the spot weld samples, the penetrating power of the laser is directly proportional to the heat input density. The weld penetration depth increased from 354 µm to 781 µm (Table 3) and weld width increased from 906 µm to 1088 µm (Table 3) as heat input density increased from 45,325.95 J/cm^2 to 362,607.62 J/cm^2 (Table 2) or as laser active time increased from 0.125 s to 1 s (Fig. 2). This general trend is in agreement with Miyagi & Zhang (2015) [4] who reported increasing weld geometry with increasing laser power and decreasing welding speed.

Table 3. Weld geometries of the line and spot weld samples.

Sample	Weld penetration depth (µm)	Weld width (µm)
LW1	763	1,000
LW2	617	967
SW1	781	1,088
SW2	712	1,021
SW3	513	985
SW4	354	906

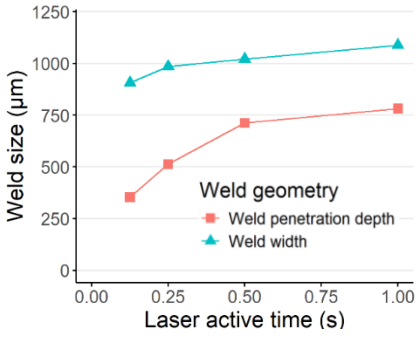

Fig. 2. Lineplot of weld penetration depth (µm) and weld width (µm) of the spot welds against laser active time (s).

[2] Laser active time of line weld = Line length ÷ Scanning speed

[3] Laser intensity (average power density) of top-hat beam = $\frac{\text{Power of laser beam}}{\text{Laser beam area}} = \frac{P_0}{\pi r^2}$

[4] Laser energy per weld (weld length for line weld; each spot for spot weld) = Laser power × Laser active time

[5] Heat input density = Laser energy per weld ÷ Weld area (area of slot for line weld; spot area for spot weld)

The weld geometries of the six welds (Fig. 3) are not purely that of conduction welds or keyhole welds, and instead resemble transition welds [5] which are an intermediate of the two weld types. The laser intensity used in this study is 3.63×10^5 W/cm^2 (Table 2). For the blue laser of 445 nm wavelength used in this study, only about 55% of the energy input is initially absorbed by the copper plate [6], translating to an effective laser intensity of 2.00×10^5 W/cm^2. Even accounting for copper's high reflectivity of light, the effective laser intensity used is sufficient to meet the minimum heat source intensity of 10^5 to 10^7 W/cm^2 required to generate a keyhole weld [3, 7]. The reason for the transition weld geometry despite meeting this threshold could be attributed to copper's high thermal conductivity (401 Wm^{-1}K^{-1}), which is 28 times higher than stainless steel and 1.7 times higher than aluminium. Energy is rapidly conducted away from the laser beam centreline to form a relatively wide fusion zone (FZ). Thus, while the laser beam has sufficient heat intensity to generate a keyhole weld, the high thermal conductivity of copper results in FZs in copper displaying geometries characteristic of transition welds.

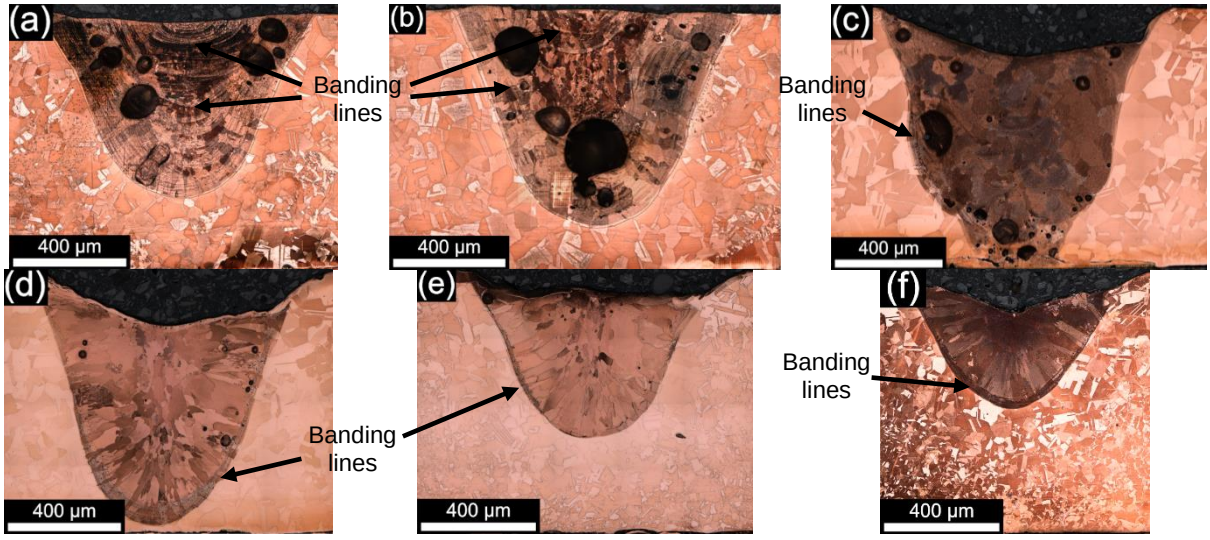

Fig. 3. Micrographs of cross-sections of (a) LW1; (b) LW2; (c) SW1; (d) SW2; (e) SW3; and (f) SW4.

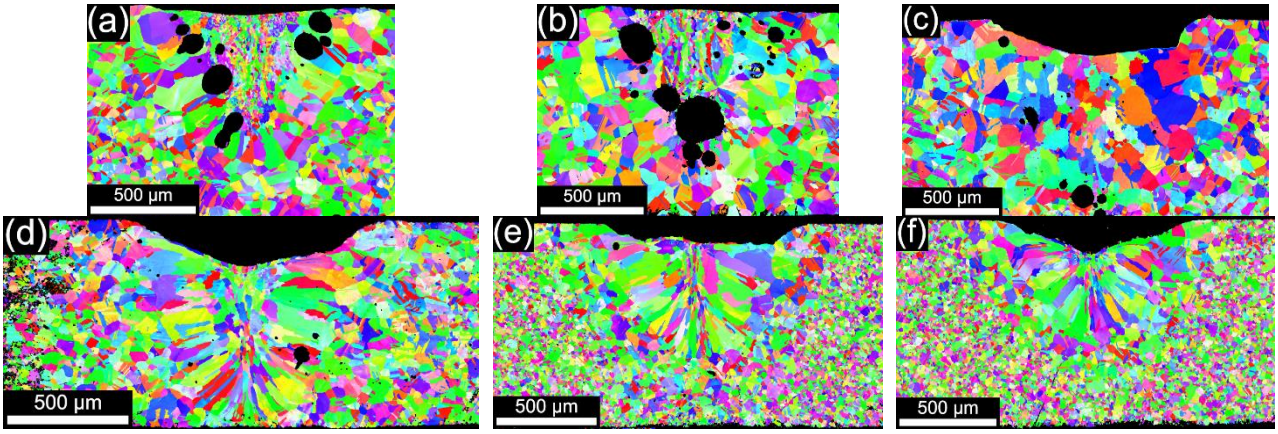

Fig. 4. EBSD images (1 µm step size) of cross-sections of (a) LW1; (b) LW2; (c) SW1; (d) SW2; (e) SW3; and (f) SW4.

3.2 Microstructure and grain size

For the line welds, banding [8] is particularly prominent throughout the entire depth of the FZs in both LW1 and LW2 (Fig. 3a and Fig. 3b). For the spot welds, banding are also observed but are generally limited to the FZ next to the fusion line (FL) (Fig. 3c to Fig. 3f). Banding is a phenomenon associated with alternating bands of varying microstructures [8]. The bands of LW2 (Fig. 5) and SW3 (Fig. 6) were investigated under the SEM to reveal the differences in microstructures. For LW2, the bands consisted of alternating equiaxed cells and elongated cells. For SW3, the bands near the FL consisted of small equiaxed cells, large equiaxed cells and elongated cells.

In all welds except SW1, there are two distinct subzones within the FZ. The middle section of the FZ is dominated by longitudinal columnar grains (LC) while the area between the LC grains and the HAZ is dominated by horizontal columnar (HC) grains [9]. The formation of the elongated grains eitherside of the more vertically oriented gains in the centre of the welds' FZ are a good indication that the high thermal conductivity of copper is affecting process performance to a good degree. Other factors could also play a role in this, and this remains to be investigated. In SW1 however, the FZ comprises of mostly large equiaxed grains in both subzones where LC and HC grains are found in the other welds. This could be explained by the heat input density of SW1 being the highest out of all spot welds, thus having the lowest cooling rate.

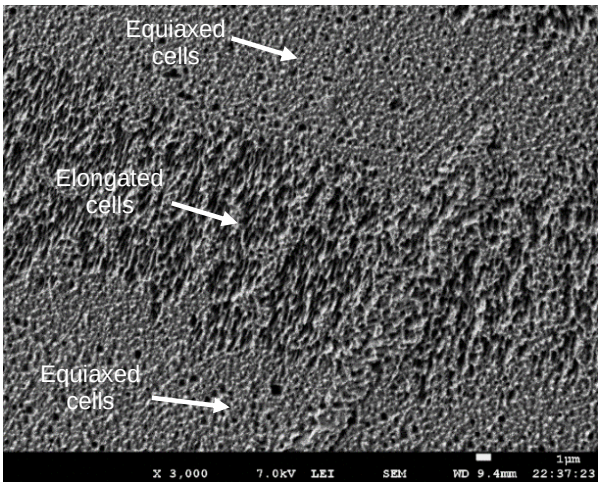

Fig. 5. SEM image (3000x magnification) of bands in LW2.

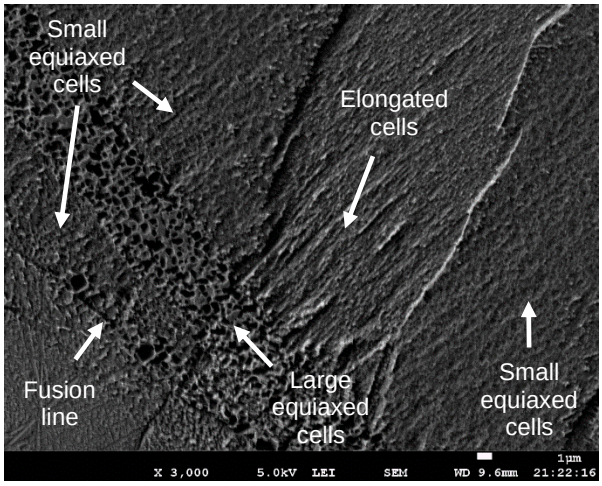

Fig. 6. SEM image (3000x magnification) of bands in SW3.

For the line welds, the average grain size of the FZ of LW1 and LW2 were 21.4 and 25.4 µm respectively (difference = 4 µm), and the average grain size outside the FZ (OFZ) of LW1 and LW2 were 50.6 and 60.8 respectively (difference = 10.2 µm). For the spot welds, the average grain size increased from 25.1 to 34.0 µm for the FZ (see next paragraph for a discussion on average grain size value for SW1's FZ) and increased from 17.1 to 47.1 µm for the OFZ as laser active time increased from 0.125 s to 1 s (Fig. 2).

In addition, SW1 has the coarsest grain structure in both the FZ and the HAZ compared to the other spot welds (Fig. 4). Again, SW1 has the highest heat input density and thus lowest cooling rate since it would take the longest to dissipate the irradiated laser energy. The longer time spent above the grain-coarsening temperature of copper in SW1 means that the grain structure of both its FZ and HAZ would be coarser than the rest of the spot welds. This is substantiated by the higher average grain size value of SW1 of the area outside the fusion zone (OFZ), which includes the HAZ, compared to the other spot welds (Fig. 7), which indicates that there is more HAZ than base material for the same EBSD scan area.

The average grain size of the FZ of SW1, however, paints a different picture where the average grain size is similar to the rest of the spot welds (Fig. 7). When comparing average grain size of the HC grain subzone, SW1 even has lower average grain sizes than the other spot welds. This apparent contradiction when comparing the qualitative data (i.e., EBSD image) and quantitative data can be attributed to the fact that a coarser grain structure would have lesser grains within a given area. In SW1's case, the large and coarse grains are fewer in number. Thus, when a relatively large number of smaller grains are included in the dataset, the definition of the boxplot (i.e., data points beyond 1.5 × IQR are deemed as outliers) would exclude many of the largest grains as outliers. This is evident in the FZ_HC beanplot (Fig. 7) where many outliers are seen above the third quartile of SW1's boxplot. For reference, the sample size (n) of grain size dataset for SW1, SW2, SW3 and SW4 are 85, 176,262, and 363 respectively.

We can thus see that heat input density is a major factor affecting grain size as well as their shape, occurring as elongated, HC or LC, or ending up mostly equiaxial. In addition, the minimum heat input density required to attain an equiaxial grain structure could be in the range of 2×10^5 to 3×10^5 J/cm^2, which is in between that of SW1 and SW2.

3.3 Hardness

For the spot welds, the Vickers microhardness (HV) of FZ is greater than the base material, which is greater than the HV of HAZ. The HV of the FZ in SW1 ranged from 84.65 to 100.79 (Fig. 8), which is significantly lower than the other spot welds which had HV of the FZ ranging from 127.79 to 172.92 (Fig. 8). This can be attributed to the coarse equiaxed grain structure of SW1, as discussed in Section 3.2, which has higher ductility compared to the elongated grain structure present in SW2, SW3 and SW4. The HV of the FZ of the line welds are similar to that of SW1, although the grain structure in the FZ consisted of elongated grains rather than the equiaxed grain structure of SW1.

In all spot welds, the HV of the HAZ generally range between 50 and 70, which are lower than the mean HV of 81.52 of the base material. In SW2, SW3 and SW4, HV values of around 150 are being observed which are well above the average of the base material. These results contrast that of Zhang et al. (2015) [9], who reported decreasing Vickers microhardness or softening of both the FZ and HAZ compared to the base material in fiber laser butt welding of T2 copper joints.

3.4 Defects

Porosity and surface voids were observed in the weld zones of all samples, except SW4 for porosity (Table 4). For the line weld samples, the diameter of the largest pore observed differed by 68 µm (Table 4) for the same heat input density of 66,677.25 J/cm^2 (Table 2). For the spot weld samples, the diameter of the largest pore observed increased from 14 µm to 134 µm (Table 4) as heat input density increased from 90,651.91 J/cm^2 to 362,607.62 J/cm^2 (Table 2). Note that no pores were observed in the

cross-section of SW4 (Table 4), which had a heat input density of 45,325.95 J/cm^2 (Table 2; Fig. 3f).

In all welds except LW2, voids of 31 µm to 183 µm (Table 4) between the weld surface and substrate surface were observed. The voids suggest that there was loss of copper material by melt spattering and/or vapourisation, which is an observation consistent with several other published studies reporting melt ejections and spattering during laser welding of copper [3, 10, 11].

Table 4. Porosity and surface voids observed in the micrographs of the line and spot weld samples.

Sample	Diameter of large pore (µm)	Height of surface void (µm)
LW1	144	33
LW2	227	Nil
SW1	134	180
SW2	44	183
SW3	14	64
SW4	Not observed	121

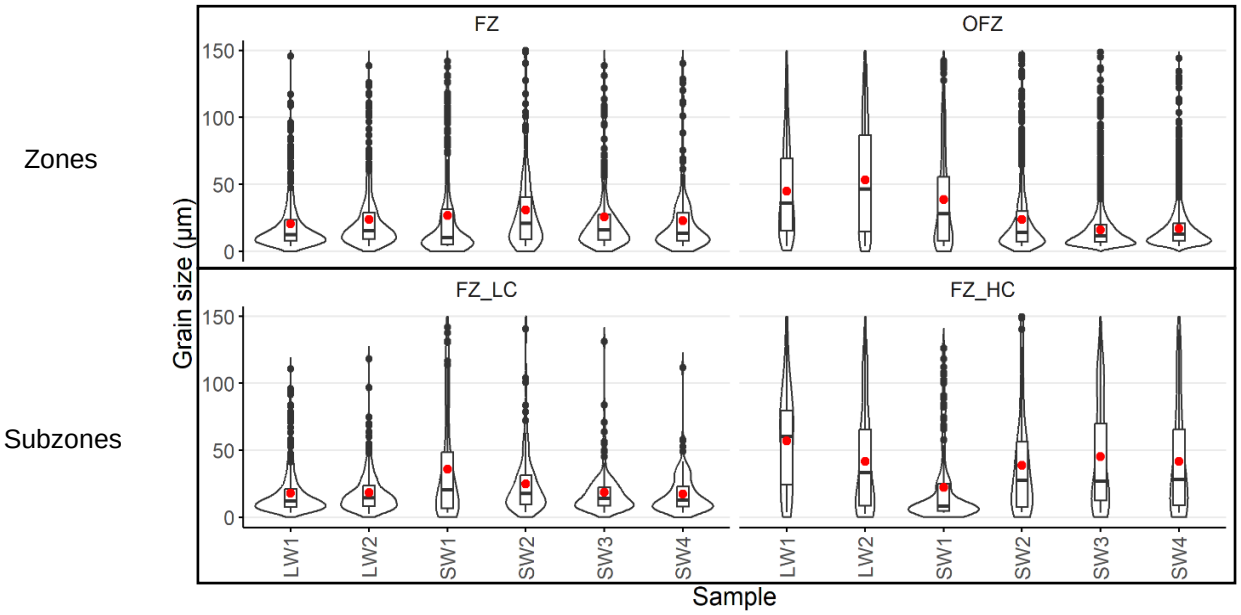

Fig. 7. Beanplot of average grain size against sample, grouped by zones: FZ = Fusion Zone; OFZ = Outside Fusion Zone; and subzones: FZ_LC = Fusion Zone (Longitudinal Columnar); FZ_HC = Fusion Zone (Horizontal Columnar). Notes: (1) Each bean represents a density trace indicating the number of grains at that grain size value. (2) Each boxplot represents the minimum, maximum, interquartile range, and median values of grain size. (3) Each circle within the boxplot represents the mean value of grain size. (4) The FZ_LC and FZ_HC subzones of SW1 are dominated by equiaxed grains—the same subzone labelling is applied to SW1 for consistency and comparison. (5) The OFZ zone includes both the HAZ and base material if the base material grains are present.

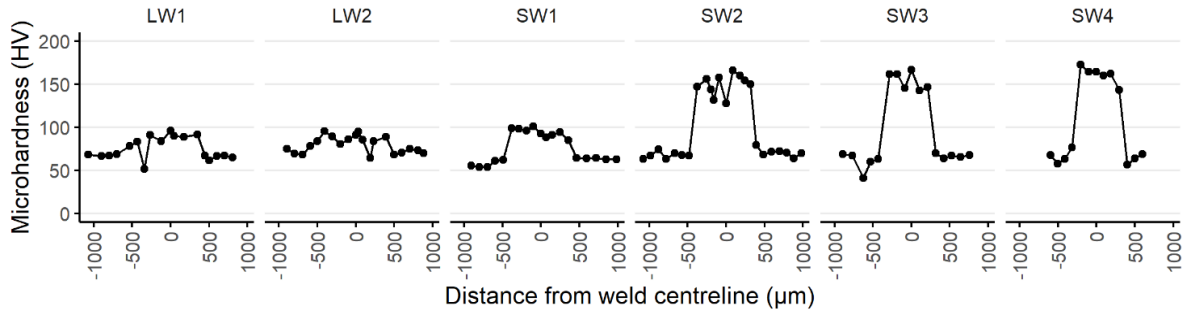

Fig. 8. Lineplot of Vickers microhardness (HV) against distance from the weld centreline (µm). Mean HV value of substrate = 81.52.

For the line welds, the pores and voids could be caused by insufficient laser power and welding speed. Miyagi & Zhang (2015) [4] investigated the spattering phenomena in laser welding of pure copper, and found that one of the factors impacting spattering is whether the molten metal load exceeds the expansion pressure from copper vapour in the keyhole weld zone. If vapour expansion pressure exceeds the molten metal load, then the upwards force exerted by the keyhole expansion promotes ejection of molten metal from the weld zone. To mitigate melt ejection or spattering, Miyagi & Zhang (2015) [4] suggested increasing the laser power or welding speed. Increasing the laser power increases the molten metal load (because of larger weld pool) faster than it increases vapour expansion pressure, and prevents the vapour expansion pressure from overcoming the molten metal load. Increasing the welding speed past the speed of weld pool formation promotes keyhole weld stability in two ways [4]: firstly it prevents the laser beam from continuously interacting with the weld pool which results in higher rates of copper vapour formation, and secondly the keyhole weld pool flow regime tends to be more stable with the melt pool flowing only backwards away from the laser movement direction which keeps the rate of copper vapour formation constant. As a reference, Miyagi & Zhang (2015) [4] used a scanning speed of 166.67 mm/s,

roughly 55.56 times the scanning speed of 3 mm/s used in this study, to minimize porosity and spattering.

For the spot welds, since the welds are stationary and the laser active time of each spot weld is longer than that of any given spot in the line weld, the weld pool mechanism for spot welds with longer laser active time is likely to be continuous interaction of the laser beam with the weld pool resulting in higher rates of copper vapour formation [4]. The expansion pressure from the copper vapour then leads to surface voids from spattering and porosity during rapid cooling arising from high thermal conductivity. Although no large pores were observed in SW4, the surface void of 121 µm is still substantial considering that the copper substrate is only 0.9 mm thick.

4 Conclusions

This study investigated the use of a top-hat CW 1.5 kW blue diode laser of 445 nm wavelength to weld a 0.9 mm copper plate to a 0.3 mm stainless steel plate. Characterisation of the welds was carried out and the main findings are:

Weld geometry. Only SW1 achieved full penetration of the copper plate (weld penetration depth of 781 µm excluding surface void depth of 180 µm), reaching the stainless steel plate although there was no melting of the steel. For the spot welds, weld penetration depth increased from 354 µm to 781 µm and weld width increased from 906 µm to 1088 µm as heat input density increased from 45,325.95 J/cm^2 to 362,607.62 J/cm^2. For the line welds, the heat input density was the same at 66,677.25 J/cm^2 but weld penetration depth differed by 146 µm and weld width differed by 33 µm.

Microstructure. For the line welds, banding is particularly prominent throughout the entire depth of the FZs. The bands consisted of alternating equiaxed cells and elongated cells. For the spot welds, banding is also observed but is generally limited to the FZ next to the FL. The bands consisted of small equiaxed cells, large equiaxed cells and elongated cells. The FZs of both line welds and spot welds (except SW1) comprise of LC grains in the middle section and HC grains in the area between the middle section and the FL. SW1, with the highest laser active time of 1 s, or highest heat input density of 362,607.62 J/cm^2, had a largely coarse and equiaxed grain structure in both the FZ and HAZ. The minimum heat input density required to attain an equiaxial grain structure could be in the range of 2×10^5 to 3×10^5 J/cm^2.

Average grain size. For the line welds, the average grain size of the FZ of LW1 and LW2 were 21.4 and 25.4 µm respectively, and the average grain size of the OFZ of LW1 and LW2 were 50.6 and 60.8 respectively (difference = 10.2 µm). For the spot welds, the average grain size increased from 25.1 to 34.0 µm for the FZ and increased from 17.1 to 47.1 µm for the OFZ as laser active time increased from 0.125 s to 1 s.

Hardness. For the spot welds, the HV of FZ is greater than the base material, which is greater than the HV of HAZ. The HV of the FZ in SW1 ranging from 84.65 to 100.79 is significantly lower than the HV of the FZ of the other spot welds ranging from 127.79 to 172.92. This is attributed to the coarse equiaxed grain structure of SW1. The HV of the FZ of the line welds are similar to that of SW1, although the grain structure in the FZ of the line welds consisted of elongated grains. The HV of the HAZ of all spot welds (50 to 70) are lower than the mean HV of 81.52 of the base material.

Defects. Porosity and surface voids were observed in the weld zones of all samples, except SW4 for porosity. For the line welds, the diameter of the largest pore differed by 68 µm for the same heat input density of 66,677.25 J/cm^2. For the spot weld samples, the diameter of the largest pore observed increased from 14 µm to 134 µm as heat input density increased from 90,651.91 J/cm^2 to 362,607.62 J/cm^2. No pores were observed in the cross-section of SW4, which had a heat input density of 45,325.95 J/cm^2. In all welds except LW2, surface voids between 31 µm to 183 µm were observed.

In summary, weld penetration depth for a 0.9 mm copper plate was inadequate with the parameters used in this study. There are indications that longer laser active time or increase in average power can help to achieve full penetration to the underlying stainless steel sheet, but care must be taken to limit the heat input and weld penetration that would negatively affect the internal components and function of the battery. We demonstrated that different microstructures and grain sizes can be attained by changing the laser process parameters with laser active time or heat input density being the most important. Further optimisation work is required to control porosity and surface voids in copper. The improved coupling of the wavelength into the material should permit applying such controls in the process using the blue laser source.

5 References

[1] A. Sadeghian, N. Iqbal, Opt. Laser Technol., **155**, p. 108415 (2022)

[2] A. Sadeghian, N. Iqbal, Opt. Laser Technol., **146**, p. 107595 (2022)

[3] S. T. Auwal, S. Ramesh, F. Yusof, S. M. Manladan, Int. J. Adv. Manuf. Technol., **96**, no. 1–4, pp. 475–490 (2018)

[4] M. Miyagi, X. Zhang, J. Laser Appl., **27**, no. 4, p. 042005 (2015)

[5] M. Chludzinski, R. E. Dos Santos, C. Churiaque, M. Ortega-Iguña, J. M. Sánchez-Amaya, Metals, **11**, no. 4, p. 640 (2021)

[6] H. Yang, X. Tang, C. Hu, S. Liu, Y. Fan, Y. Xiao, G. Lu, Q. Wang, G. Chen, P. Xing, H. Tan, Z. Guo, Z. Niu, J. Laser Appl., **33**, no. 3, p. 032018 (2021)

[7] J. F. Lancaster, *Metallurgy of Welding*. Dordrecht: Springer Netherlands (1980)

[8] E. A. Torres, L. H. R. Apolinario, H. R. Araujo, I. B. M. Picchi, T. F. A. Santos, Int. J. Adv. Manuf. Technol., **112**, no. 7–8, pp. 2327–2339 (2021)

[9] L.-J. Zhang, G.-F. Zhang, J. Ning, X.-J. Zhang, J.-X. Zhang, Mater. Des., **88**, pp. 720–736 (2015)

[10] S. Liebl, R. Wiedenmann, A. Ganser, P. Schmitz, M. F. Zaeh, Phys. Procedia, **56**, pp. 591–600 (2014)

[11] L. Wang, X. Li, M. Gao, X. Zeng, J. Manuf. Process., **27**, pp. 207–213 (2017)